ACS OMEGA

Open Access

http://pubs.acs.org/journal/acsodf

Article

Spontaneous Combustion Characteristics of Activated Carbon Modified via Liquid Phase Impregnation during Drying

Qing-en Li, Bing J. Zhang,* Shu-shen Lyu, and Zhiwen Qi

Cite This: *ACS Omega* 2023, 8, 32752−32764

Read Online

ACCESS | Metrics & More | Article Recommendations

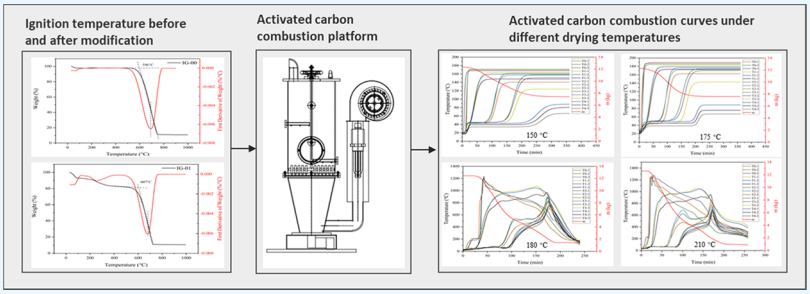

ABSTRACT: Spontaneous combustion characteristics are important issues for the safe operation of the wet-modified activated carbon drying process. The spontaneous combustion characteristics of activated carbon modified via liquid phase impregnation were fully investigated in this study. The modified activated carbon was prepared using columnar activated carbon and 4-amino-1,2-butanediol solution. Physical properties and surface functional group analyses were performed for activated carbon before and after modification. The ignition temperature of activated carbon before and after modification was then characterized using the methods of GB/T20450−2006, thermogravimetry−derivative thermogravimetry (TG-DTG), and TG−mass spectrometry (TG-MS). At the same time, the activation energy of activated carbon before and after modification was calculated by using thermodynamic analysis. Furthermore, a new self-designed test platform was introduced to investigate the spontaneous combustion characteristics of wet-modified activated carbon under the drying temperatures of 150, 175, 180, and 210 °C. The results show that the specific surface area of Brunauer, Emmett, and Teller (BET) is decreased by 368 $m^2 \cdot g^{-1}$, the total volume of pore size is decreased by 0.17 $cm^3 \cdot g^{-1}$, and the content of oxygen-containing functional groups is decreased by 0.071 mmol/g compared with row activated carbon. The ignition temperatures of the sample before modification characterized by the three methods are 483, 596, and 599 °C, respectively. The ignition temperatures of the sample after modification are 489, 607, and 611 °C, respectively. The activation energy of the modified activated carbon is increased by 35 kJ/mol compared to the original activated carbon. It is concluded that the temperature that triggers the modified activated carbon combustion during the drying process is between 175 and 180 °C, and the heat is mainly gathered at the longitudinal center of the combustion chamber through the investigation of spontaneous combustion experiments. The results in this study can contribute to safe production to prevent combustion in the process of modifying activated carbon during the drying process.

1. INTRODUCTION

Formaldehyde is a highly toxic indoor contaminant that can dramatically impact human health.[1] Various techniques have been introduced for removing formaldehyde from an indoor atmosphere.[2] Adsorption is low in cost and can be easily applied to operation.[3] Activated carbon has been widely used as an adsorbent for removing pollutants due to its large specific surface area, well-developed pore structure, abundant functional groups, and reusability.[4,5] Activated carbon has significant advantages in the treatment of gaseous pollutants, such as formaldehyde, toluene, benzene, etc.[6] Furthermore, activated carbon is relatively cheaper than other adsorbates and low investment is required.[7] The surface functional groups and pore structures of activated carbon are the key factors to impact its adsorption performance to formaldehyde.[8]

Optimizing the pore structure and surface functional groups by changing the carbonaceous materials of precursors, activation methods, and manufacturing process parameters can improve activated carbon adsorption performance to formaldehyde.[9] Several studies have shown that modifying activated carbon can

Received: May 25, 2023
Accepted: August 18, 2023
Published: August 29, 2023

significantly improve its physical and chemical characteristics, which in turn enhance adsorption selectivity and capacity.[10] Activated carbon modification is generally implemented using acid treatment,[11] base treatment,[12] microwave irradiation,[13] ozone oxidation,[14] impregnation with hydrophilic chemicals, and grafting of hydrophilic functional groups connected to the activated carbon surface.[15,16] Acid treatment or base treatment is usually performed by immersing the activated carbon in different solutions, which is followed by filtration and drying. However, the drying process of wet-modified activated carbon is extremely prone to cause fires if the temperature increase due to heat accumulation exceeds its ignition temperature.[17,18] The increasing number of applications in the activated carbon modification industry and the frequent occurrence of combustion in the process of modifying activated carbon have necessitated additional studies on the safety research and combustion prevention.[19]

The combustion in the process of modifying activated carbon is related to the properties of activated carbon, solvent properties of modified chemicals, drying gas, drying temperature and time, atmosphere flow, fluidization, and dust and moisture emissions in the drying process.[20−23] Spontaneous combustion of activated carbon generally occurs when its surface undergoes an exothermic reaction due to oxidation.[24] Onifade's study indicated that the spontaneous combustion of coal and coal-derived activated carbons is the results of carbon oxidation.[25] The spontaneous combustion of activated carbon from coal is affected by factors such as deposition temperature, rank, and maceral composition of coal feedstock as well as ash content.[26] Nugroho argued that pore sizes play a crucial role in the oxidation process, as oxygen consumption during low-temperature oxidation is determined by their penetration into the pore structure of activated carbon.[27] Jia's studies show that the particle size of coal is an important index affecting the coal oxidation; the smaller the particle size, the larger specific surface area, and the larger the contact area between coal and oxygen, resulting in a lower activation energy for the reaction and easier oxidation of the coal samples.[28]

The nature of spontaneous combustion of coal or coal-derived activated carbon is the reaction between the active functional groups and oxygen, and the difference of the microstructure leads to the difference of macrocharacteristics.[29] The more the surface-active groups of the same mass is in contact with oxygen, the faster the oxidation heating rate will be.[28] The surface functional groups of activated carbon have been investigated to study the behaviors of spontaneous combustion. Niu believe that the spontaneous combustion of coal should be closely related to functional groups.[30] Jayabalan found that increasing the content of surface-oxygenated groups augmented the reactivity of activated carbons.[31] Xu elucidated the reaction mechanism of spontaneous coal combustion by characterizing the reaction of free radicals and functional groups during low-temperature oxidation of coal.[32] Tang determined that the spontaneous combustion tendency of preoxidized lignite is closely correlated to the treatment time and temperature.[33] Zhang observed that the formation and consumption of hydroxyl, carbonyl, carboxyl, and other substituted aromatic hydrocarbons play a crucial role in low-temperature oxidation.[34] Guo investigated the changes in the key functional groups and thermal parameters of coal after preoxidation, which altered the characteristic temperature and activation energy.[35] Different methods have been established to predict the spontaneous combustion liability of coal and other carbonaceous materials. The point of initial oxidation (PIO), crossing point temperature (CPT), spontaneous ignition temperature (SIT), and activation energy are major indicators in the process of activated carbon or coal spontaneous combustion to evaluate their thermal stability. Gao characterized the spontaneous combustion tendency of metamorphic coal through CPT and activation energy calculated from the oxidation kinetics experiment.[36] Yang performed a thermal analysis to characterize the reaction of coal with different pyrite contents and employed the Flynn−Wall−Ozawa method to calculate the activation energy of coal with different pyrite contents.[37] Guo analyzed the influence of the drying process on the coal by comparing activation energies and functional groups of immersed coal with different drying degrees to those of raw coal.[38]

Preventing and mitigating accidents caused by process-related hazards through inherent safe design is one of the most effective strategies for avoiding accidents in the field of process safety management. Therefore, many scholars currently investigate the characteristics of spontaneous combustion through self-built spontaneous combustion experimental platforms or laboratory experiments so as to prevent spontaneous combustion disasters.[39] Du carried out temperature-programed experiments on row coal samples and coal samples with inhibitors.[40] Ma designed an experimental platform comprising a longwall gob to investigate the methane migration process induced by the spontaneous combustion of coal.[41] Zhu proposed a general inherent safety assessment tool (ISAT) to evaluate the inherent safety level at the early design stage of the chemical process.[42] Computational fluid dynamics (CFD) is a numerical method with the advantages of low risks, low cost, and high computational efficiency compared to an experiment study.[43] Malendowski and Glema conducted a CFD-based model to predict the fire action.[44] Shibani used CFD simulation to assess the safety of multiple hydrogen fires in confined areas.[45] At present, different CFD codes have been developed for the simulation of fire or explosion, such as FLACS, FLUENT, and FDS.

Understanding the factors that contribute to the spontaneous combustion of activated carbon and developing methods to prevent combustion in the process of modification are crucial for activated carbon modification safe manufacturing. However, the existing research has focused on the safety aspects of spontaneous combustion of activated carbon before and after its modification, and the spontaneous combustion characteristics of wet-modified activated carbon during the drying process has not been fully investigated. Therefore, it is necessary to study the actual development process of the spontaneous combustion of wed-modified activated carbon during the drying process. In this study, a comprehensive characteristic of activated carbon before and after modification is elucidated by investigating the surface functional groups, testing the ignition temperature, and calculating the activation energy based on thermal dynamics; a new self-designed test platform is then introduced to develop the critical drying temperature and time that trigger the combustion of wet-modified activated carbon. The temperature spread and mass change of activated carbon from the time when drying begins to the end of combustion are monitored and observed in the self-designed test platform.

2. EXPERIMENTAL METHODS AND CHARACTERIZATION

2.1. Experimental Apparatus and Materials. Coal-based columnar activated carbon (HH-70, China) with a diameter of 2

https://doi.org/10.1021/acsomega.3c03563
ACS Omega 2023, 8, 32752−32764

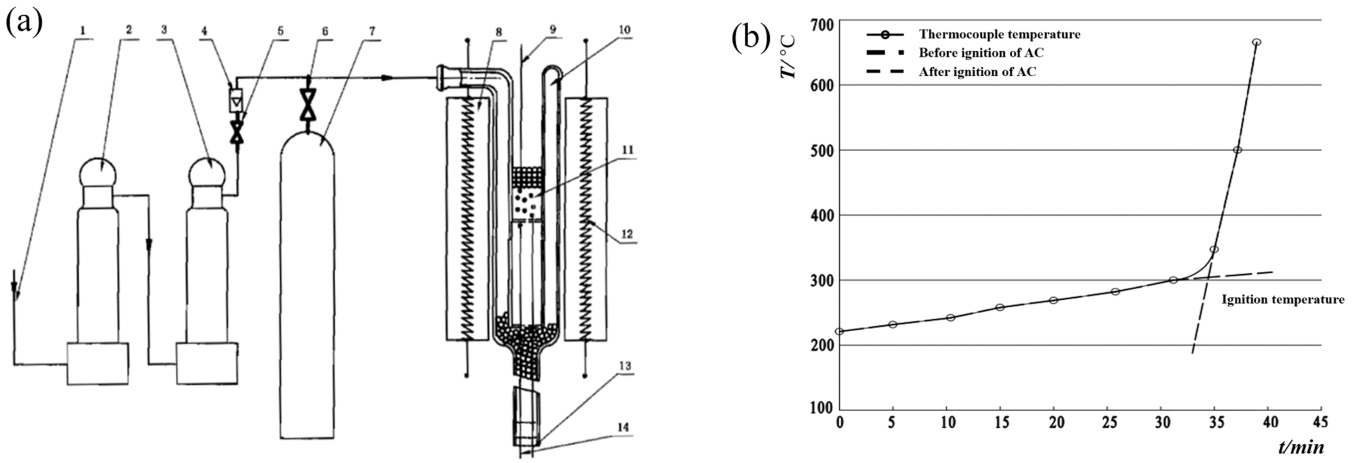

Figure 1. Layout and method to determine the activated carbon ignition temperature. (a) Layout of the ignition temperature test device (1, air source; 2, air dryer; 3, activated carbon; 4, flowmeter; 5, air switch; 6, nitrogen switch; 7, nitrogen cylinder; 8, heating jacket; 9, thermocouple T-2; 10, quartz combustion pipe; 11, sample; 12, electric heating wire; 13, thermocouple T-1; and 14, thermocouple T-3). (b) Method to determine the activated carbon ignition temperature.

mm and a carbon tetrachloride adsorption value of 70 was used as the raw material after dust removal. The 4-amino-1,2-butanediol solution was of analytical grade and prepared using pure water filtered via reverse osmosis.

2.2. Preparation of Modified Activated Carbon. One kg amount of HH-70 activated carbon is immersed in 2 kg of 4-amino-1,2-butanediol solution with a mass concentration of 12.0%, and the resulting solution is mixed well to ensure full contact between the activated carbon and adsorbate. The impregnated activated carbon is sucked to remove the residual liquid on the surface and then is dried on the self-designed combustion test platform; the moisture content of the modified activated carbon after drying is controlled at 9%. The activated carbon samples before and after modification are named IG-00 and IG-01, respectively.

3. PHYSICAL AND CHEMICAL PROPERTIES OF ACTIVATED CARBON BEFORE AND AFTER MODIFICATION

3.1. Industrial Analysis and Elemental Analysis. Industrial and elemental analyses are performed on samples IG-00 and IG-01. The industrial analysis is performed according to the gravimetric method based on the GB/T 3521−2008 standard, and the content of nonmetallic elements is determined using an elemental analyzer (Unicube, Elementar).

3.2. Characterization of Physical Properties of Activated Carbon. A pore size distribution meter (ASAP 2460, Micromeritics Instrument Corp.) is used to test the specific surface area and pore size distribution of samples IG-00 and IG-01. The specific surface area and pore size distribution are determined using the Brunauer, Emmett, and Teller (BET) method based on the GB/T 19587−2017 standard.

3.3. Characterization of Functional Groups of Activated Carbon before and after Modification. The types of functional groups on the activated carbon surface are determined by using a Fourier transform infrared spectrometer (TENSOR 27, BRUKER). A tableting method is employed, wherein 5 mg of sample and 250 mg of pure KBr are pulverized and evenly placed in the mold, after which the mold is gradually pressurized up to 20 MPa by using a hydraulic press. The sample is pressed into a transparent sheet and analyzed using the Fourier transform infrared (FT-IR) transmission mode to obtain its infrared absorption spectrum.

The amount of oxygen-containing functional groups is determined using the Boehm method. Two activated carbon samples with a mass of 1 g are first weighed using an electronic balance, after which they are inserted into conical flasks with a volume of 100 mL. Subsequently, 25 mL of standard solutions of NaOH, Na_2CO_3, and $NaHCO_3$ with a concentration of 0.05 mol/L are added. After the resulting solution was mixed for 24 h, filtration is performed, and the filtrate is collected and washed with distilled water. By using methyl red as the end point indicator, the unreacted lye in the filtrate is titrated to the end point using a 0.05 mol/L HCL standard solution. Herein, NaOH is used for titrating the carboxyl group, lactone group, and phenol group. Meanwhile, $NaHCO_3$ is used for titrating the carboxyl group, and Na_2CO_3 is used for titrating the carboxyl group and lactone group. The total amounts of basic functional groups are calculated using the amount of 0.1 mol/L HCL consumed.

3.4. Ignition Temperature of Activated Carbon before and after Impregnation Modification. An activated carbon ignition temperature determination method was introduced by GB/T20450−2006, and the ignition temperature is defined as the minimum temperature at which activated carbon combustion occurs under the specified conditions. The thermocouple tests the temperature before and after ignition of activated carbon; the intersection of the temperature curve extension line before the sharp heating and the temperature curve extension line after the sharp heating of activated carbon is defined as the ignition temperature. Figure 1 shows the layout of the device used for determining the ignition temperature of activated carbon and the method to determine the activated carbon ignition temperature. The sample is loaded onto the combustion tube at 25 mm, and the carbon layer covers the quartz beads with a height of 15 mm to prevent the carbon layer from fluidizing. To control the temperature's rise rate, the tip of thermocouple T-1 is placed at the upper three-quarters of the sample and the tip of thermocouple T-2 is placed at the lower three-quarters of the sample. Subsequently, the air switch is turned on and clean and dry air is provided at a flow rate of 20 L/min for 1 h. Then, the air flow rate is adjusted to 14.7 ± 0.3 L/min, and the device begins to heat up automatically. The temperature increases at a rate of

https://doi.org/10.1021/acsomega.3c03563
ACS Omega 2023, 8, 32752−32764

10 °C/min. When the air temperature reaches 150 °C, the device automatically alters the heating rate to 2−3 °C/min; this rate is maintained until the carbon layer catches fire, after which the device automatically stops providing heat and turns off the air switch.

3.5. Thermogravimetric Analysis of Activated Carbon before and after Impregnation. A thermogravimetry−differential scanning calorimetry synchronous thermal analyzer (TGA/DSC3+, METTLER) is used for conducting a kinetic test by supplying dry air as the carrier gas at a constant flow rate of 50 mL/min. Different heating rates (5, 10, 15, 20, and 25 °C/min) from room temperature to 1200 °C are used to test the weight loss of IG-00 and IG-01 samples during the oxidation heating process, after which the activation energy is calculated.

3.6. Combustion Experiments of Modified Activated Carbon Performed on a Test Platform. The combustion platform used for activated carbon has been developed based on an industrial drying equipment. Thus, it can be used not only for drying impregnated activated carbon but also for simulating the combustion of modified activated carbon. The platform comprises a cylindrical combustion chamber (Φ = 266 mm, H = 525 mm), a fan, a heater, a thermocouple, a mass sensor, an auxiliary pipeline, a bracket, and an exhaust gas discharge system. The structural design of the platform is shown in Figure 2.

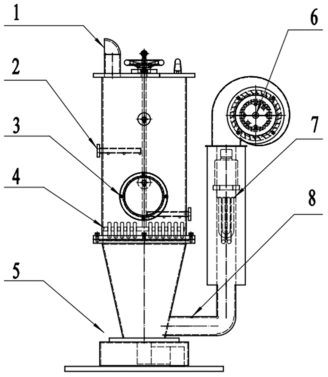

Figure 2. Platform used for activated carbon combustion (1, air outlet; 2, thermocouple bracket; 3, observation window; 4, mixing rake; 5, electronic balance; 6, fan; 7, heater; and 8, temperature controller).

A total of 15 thermocouples are installed in the combustion chamber, and the layout of these thermocouples is shown in Figure 3. Among them, three are installed at the bottom metal mash of the combustion chamber, where the activated carbon is first heated: T0−1, T0−2, and T0−3. Four brackets are spirally installed on the bottom of the combustion chamber, with the two adjacent brackets forming an angle of 90°; these are named from bottom to top as brackets 1, 2, 3, and 4. Three thermocouples are installed on each bracket, and the thermocouples installed on bracket 1 are named T1−1, T1−2, and T1−3 from the centerline to the wall of the combustion chamber. Similarly, the thermocouples on bracket 2 are named T2−1, T2−2, and T2−3; the thermocouples installed on bracket 3 are named T3−1, T3−2, and T3−3; and the thermocouples installed on bracket 4 are named T4−1, T4−2, and T4−3. Meanwhile, the mass of activated carbon in the combustion chamber is represented as m.

The fan air volume of the combustion experiment platform is set to 75 m^3/h. Subsequently, the fan, heater, thermocouple, and mass sensor are switched on under different experimental conditions. 12.22 kg of a wet-impregnated activated carbon sample (IG-01) is laid flat inside the combustion chamber (mass error of ±0.1 g), and it is required to be compact and even. Table 1 shows experiments A, B, C, and D which are performed under continuous heating at drying temperatures of 150, 175, 180, and 210 °C until the activated carbon started burning. The criterion for judging the combustion of activated carbon is that the temperature of activated carbon in the combustion chamber rose rapidly and exceeded 500 °C.

Table 1. Activated Carbon Combustion Experiment Protocol

experiment no.	drying temperature (°C)	drying time (s)
A	150	until the weight of activated carbon no longer changes
B	175	until the weight of activated carbon no longer changes
C	180	until the weight of activated carbon no longer changes
D	210	until the weight of activated carbon no longer changes

4. EXPERIMENTAL RESULTS AND ANALYSIS

4.1. Results of Industrial and Elemental Analyses. The results of the industrial and elemental analyses are shown in Table 2. The industrial analysis revealed that the volatile content of activated carbon is increased significantly after modification, and the fixed carbon content is decreased to a certain extent. At the same time, the elemental analysis revealed that the C element content of the modified activated carbon is significantly reduced, whereas the N, O, and H contents are increased. This is because the activated carbon adsorbed the adsorbate after

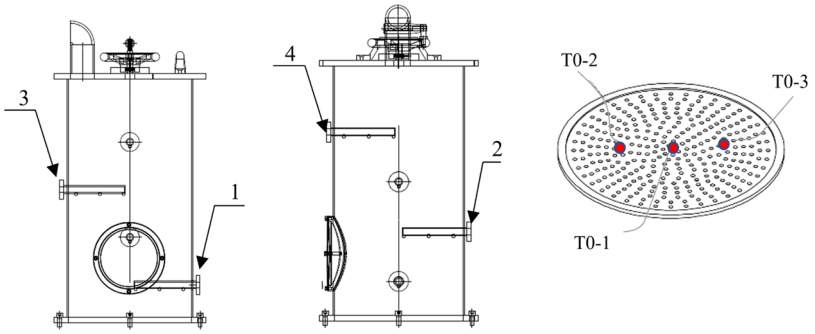

Figure 3. Thermocouple layout of the combustion platform (1, thermocouple bracket 1; 2, thermocouple bracket 2; 3, thermocouple bracket 3; and 4, thermocouple bracket 4).

https://doi.org/10.1021/acsomega.3c03563
ACS Omega 2023, 8, 32752−32764

Table 2. Proximate Analysis of Elements in Granular Activated Carbon (%)

	industrial analysis				elemental analysis				
sample	moisture	ash	volatile	fixed carbon	C	H	O	N	S
IG-00	3.4	11.9	1.3	83.4	86.4	0.5	5.1	0.4	0.4
IG-01	8.9	9.9	9.7	71.5	66.1	1.4	8.3	2.1	0.2

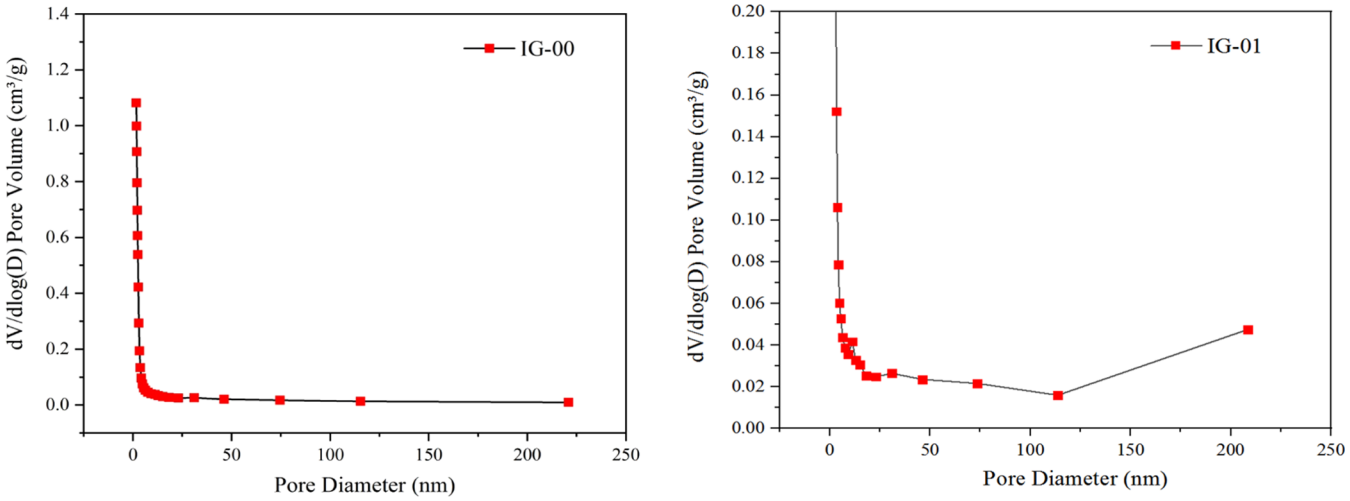

Figure 4. Pore size distributions of samples IG-00 and IG-01.

modification, and its total mass is increased by approximately 30%. The mass of C elements does not change before and after modification, while the mass of N, H, and O elements per gram of activated carbon is increased significantly after modification. This also indicates that the solvent is loaded on the activated carbon through the liquid phase impregnation.

4.2. Analysis of the Physical Properties of Activated Carbon. The specific surface area and pore size distribution are depicted in Figure 4 and Table 3, respectively. Table 3 shows

Table 3. Pore Size Distribution of the Activated Carbon Samples

sample	S_{SP} ($m^2 \cdot g^{-1}$)	S_{BET} ($m^2 \cdot g^{-1}$)	V_{tot} ($cm^3 \cdot g^{-1}$)	V_{mic} ($cm^3 \cdot g^{-1}$)	d_p (nm)
IG-00	1083	1122	0.57	0.39	2.05
IG-01	698	736	0.40	0.24	2.15

that the single-point specific surface area, BET surface area, total pore volume, and micropore pore volume of the modified activated carbon are lower than those observed before modification. This is because 4-amino-1,2-butanediol is loaded on the surface and pores of the activated carbon. Meanwhile, some micropores are oxidized and corroded into mesopores or macropores. The reduction in the specific surface area and micropore volume of the modified activated carbon is related to the type, concentration, and impregnation of the solution.

4.3. Analysis of Functional Groups on the Activated Carbon Surface. Figure 5 shows the infrared spectrogram of the sample, and the titration results are listed in Table 4. Figure 5 reveals that activated carbon before and after modification comprises the following groups: C═O, C−O, C−H, O−H, N−H, −C═O, aromatic ring C═C, possibly C═S, NO_2, and SO_3H. The samples may also contain abundant oxygen-containing groups such as phenols, alcohols, carboxylic acids, amines, hydrocarbons (saturated and unsaturated), ethers, or esters. Based on the relative intensity of FT-IR spectra, the

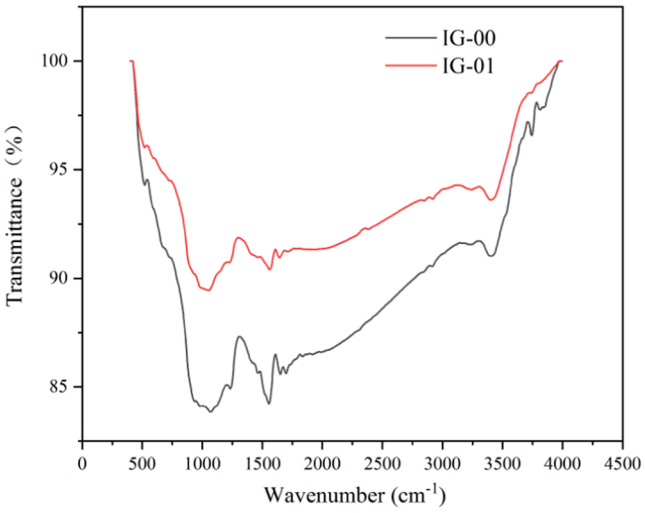

Figure 5. IR spectra of activated carbon samples.

Table 4. Results of the Boehm Titration (mmol/g)

sample	carboxyl	lactonic group	phenolic hydroxyl	total oxygen-containing functional groups
IG-00	0.509	0.023	0.080	0.602
IG-01	0.483	0.013	0.025	0.531

content of oxygen-containing functional groups in IG-01 is lower than that in IG-00.

4.4. Analysis of Activated Carbon Ignition Temperature. The ignition temperature of activated carbon is usually determined by the thermogravimetry−derivative thermogravimetry (TG-DTG) extrapolation method. On the DTG curve, the peak point is taken as a vertical line to intersect the TG curve at a point, and the tangent line to the TG curve is crossed over this point. The point where the tangent line parallels the initial weight loss of the TG curve is the ignition point, and the

https://doi.org/10.1021/acsomega.3c03563
ACS Omega 2023, 8, 32752−32764

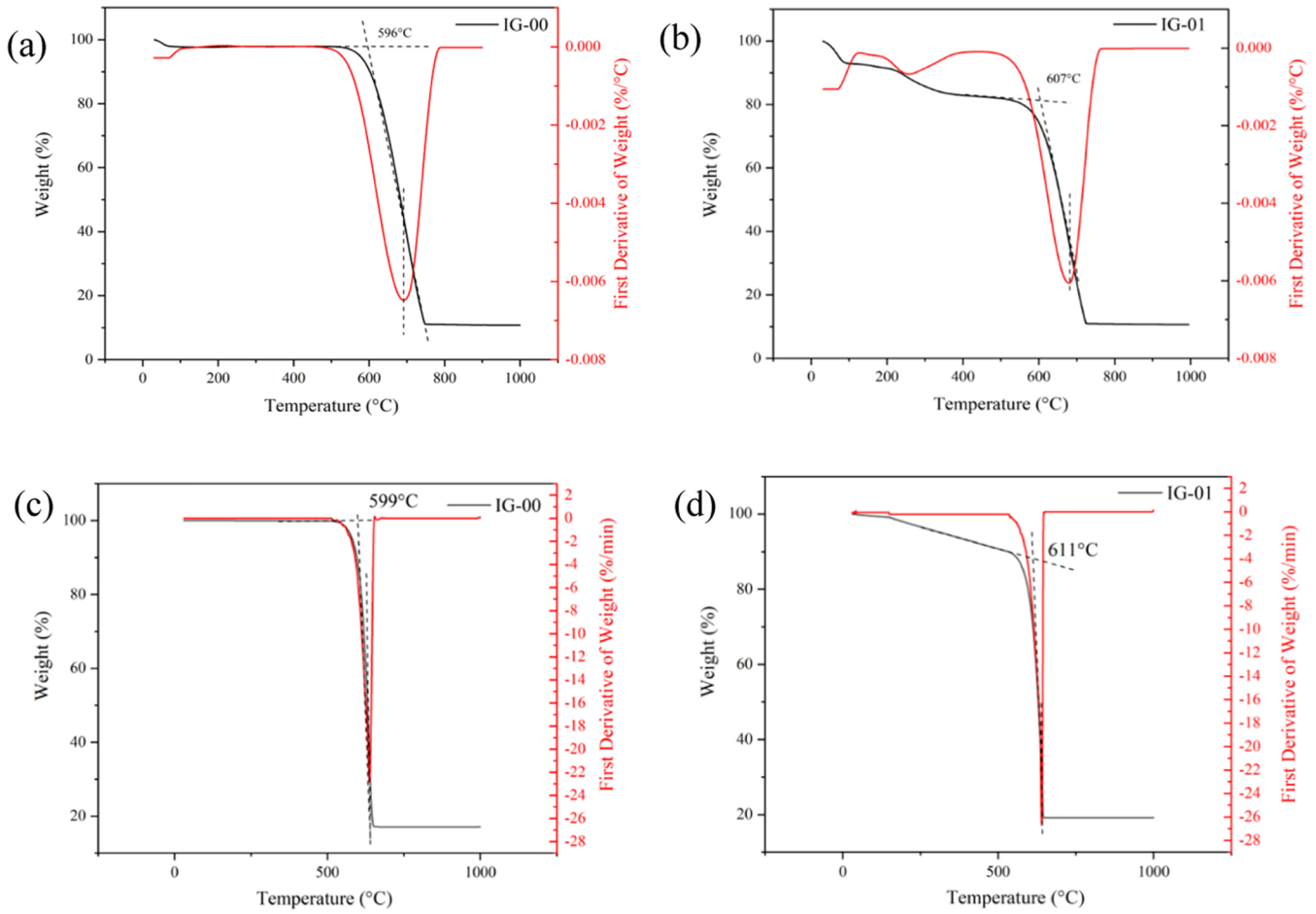

Figure 6. Ignition temperature. (a) Ignition temperature of activated carbon IG-00 characterized by the TG-DTG curve; (b) the ignition temperature of activated carbon IG-01 characterized by the TG-DTG curve; (c) the ignition temperature of activated carbon IG-00 characterized by the TG/MS curve; and (d) the ignition temperature of activated carbon IG-01 characterized by the TG/MS curve.

corresponding temperature is the ignition temperature.[44] The method of TG-mass spectrometry (TG/MS) to determine the activated carbon ignition temperature is essentially the same approach compared to the TG-DTG extrapolation method; TG/MS is a technique for combining thermogravimetric and mass spectrometry, which can generate a TG-DTG curve. The ignition temperature of activated carbon IG-00 and IG-01 has been characterized using TG-DTG and TG/MS curves in Figure 6. Table 5 shows the ignition temperatures characterized using

Table 5. Ignition Temperatures were Determined Using Different Methods (°C)

sample	GB/T20450−2006	TG-DTG	TG/MS
IG-00	483	596	599
IG-01	489	607	611

GB/T20450−2006, TG-DTG, and TG/MS. All three methods reveal that the ignition temperature of IG-01 is greater than that of IG-00, and the thermal stability of IG-01 is greater than that of IG-00; this indicates that the modification affects the ignition temperature of activated carbon. Furthermore, the contents of oxygen-containing functions such as carboxyl, lactone, and hydroxyl groups in IG-01 reduce after modification, which helps improve the thermal stability of activated carbon.

4.5. Thermal Decomposition and Thermodynamic Analysis of Activated Carbon. *4.5.1. Analysis of the Thermal Decomposition Process.* Figure 7 shows the TG and DTG curves of activated carbon samples at a heating rate of 10 °C/min. T_i,T_f,T_{eo},T_{ef}, and T_p are the characteristic physical quantities of the pyrolysis process. Initial temperature (T_i), which represents the first point that deviates from the TG curve, was determined by extrapolating the starting quasi-baseline. Meanwhile, the final temperature (T_f), which represents the last point that deviates from the TG curve, has been determined by extrapolating the final quasi-baseline. T_{eo}, which represents the temperature observed at the extrapolated starting point, is the point at which the tangent line made by extrapolating the starting quasi-baseline of the TG curve intersects with the inflection point of the TG curve step. Meanwhile, T_{ef}, which represents the final extrapolated temperature, is the point at which the tangent line made by extrapolating the final quasi-baseline of the TG curve intersects with the inflection point of the TG curve step. The temperature at which the mass change rate is maximized can be determined using the DTG curve, which indicates the temperature corresponding to the peak value of the DTG curve (represented by T_p). Table 6 shows the physical quantities determined using TG-DTG when the pyrolysis temperature is increased from 30 to 1000 °C under a heating rate of 10 °C/min.

Figure 7 reveals the following results: (1) The oxidative pyrolysis characteristic curves of the two samples are similar, with IG-01 being the first to undergo pyrolysis. (2) The first

https://doi.org/10.1021/acsomega.3c03563
ACS Omega 2023, 8, 32752−32764

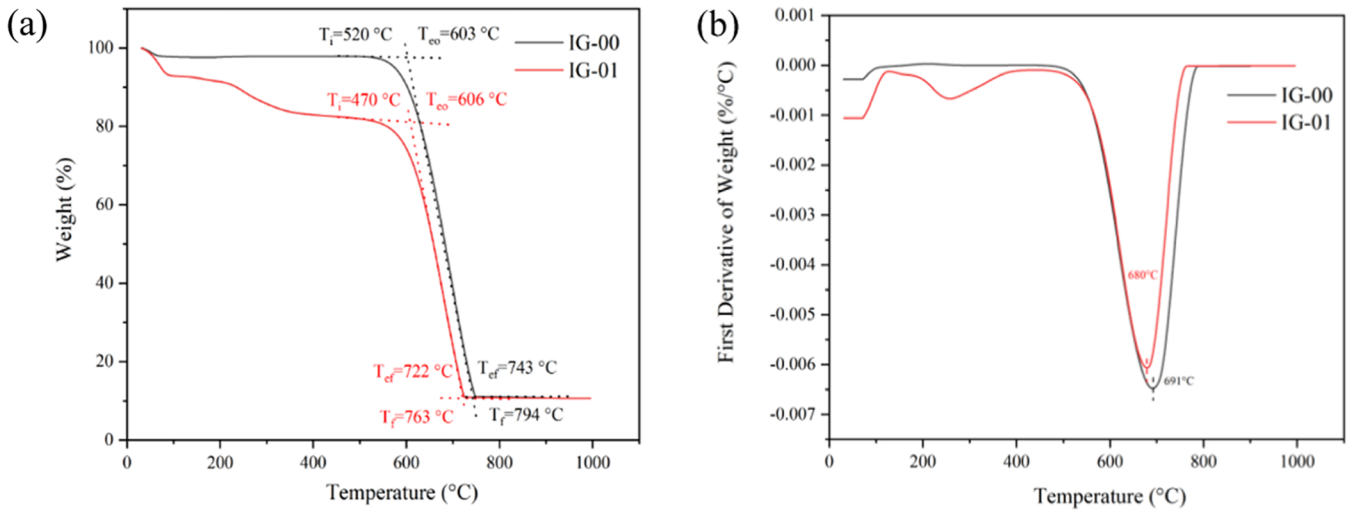

Figure 7. TG and DTG curves of activated carbon samples: (a) TG curve of activated carbon IG-00 and IG-01; (b) DTG curve of activated carbon IG-00 and IG-01.

Table 6. Physical Characteristics of Activated Carbon Samples (°C)

sample	T_i	T_f	T_{eo}	T_{ef}	T_p
IG-00	520	794	603	743	691
IG-01	470	763	606	722	680

weight loss step of the two samples occurred before 90 °C, and the IG-01 sample lost the most weight (7.3%) mainly because of its high initial moisture content. As the pyrolysis temperature increases, the pyrolysis of IG-00 ceases after weight loss and the residual mass becomes stable; IG-01 undergoes weight loss two more times, with the second and third weight loss being 10.4 and 71.6%, respectively. (3) As the temperature rises during pyrolysis, the amount of oxygen adsorbed by the activated carbon functional groups reaches its maximum value. Subsequently, the molecular structure of activated carbon is damaged and cracked, activated carbon starts to burn, and the corresponding temperature is recorded as the ignition temperature. The DTG curves reveal that the maximum weight loss occurred at 691 and 680 °C. Meanwhile, the functional and volatile groups on the activated carbon surface undergo a violent oxidation reaction. The weight loss curve tends to become flat after pyrolysis, and the residual masses of IG-00 and IG-01 seem comparable.

4.5.2. Thermodynamic Analysis of Activated Carbon before and after Modification. Figure 8 shows the TG and DTG curves at different heating rates as well as the conversion rate curves of IG-00 and IG-01. The TG and DTG curves of the two samples reveal the following results: (1) The changes in the TG curves of the samples are basically the same at different heating rates. The weight loss process is evident in the curves under five heating rates. (2) The TG curve shows that the initial decomposition temperature increases gradually. As the heating rate increases, the TG curve moves to the high-temperature region as a whole. This is because activated carbon has low thermal conductivity and weak heat transfer capacity, which leads to a slow increase in the internal temperature of the activated carbon. (3) The DTG curve reveals that when the heating rate increases, the temperature at which the mass change rate is maximum gradually increases; this result is also observed due to the low thermal conductivity and weak heat transfer capacity of activated carbon. During pyrolysis, functional and volatile groups on the sample surface undergo pyrolysis and violent oxidation reactions.

The Flynn−Wall−Ozawa (FWO) method was used along with the peak value of the DTG curve to calculate the activation energy E from the TG curve derived under different heating rates β according to the thermogravimetric experiment.[48] According to the FWO method, the expression is written as in eq 1.

$$\lg(\beta) = \lg\left[\frac{AE}{R\cdot g(\alpha)}\right] - 2.315 - 0.4567\frac{E_a}{R}\cdot\frac{1}{T} \quad (1)$$

where A is the prefactor in s^{-1}, E_a is the activation energy in kJ/mol, and R is the ideal gas constant whose value is 8.314.

For data obtained from nonisothermal thermogravimetric experiments, α is defined as

$$\alpha = \frac{m_0 - m_T}{m_0 - m_\infty} \quad (2)$$

where m_0 is the initial mass at the starting temperature, m_T is the mass when the temperature is T, and m_∞ is the final mass at the final temperature of the reaction.

When the conversion rate is constant, $g(\alpha)$ can be regarded as a constant; thus, the value of $\lg[AE/(R\cdot g(\alpha))]$ 2.315 is constant. Accordingly, the plot of $\lg(\beta)$ against $1/T$ results in a straight line, and activation energy can be calculated from this plot. By taking the reciprocal of the peak temperature T_p corresponding to the DTG curve under four different heating rates as the abscissa and considering $\lg(\beta)$ as the ordinate, plots of $\lg(\beta)$ against $1/T_p$ are obtained and linear fitting is performed to obtain a straight line; the slope of the straight line is $-0.4567\ Ea/R$, and the intercept is $\lg[AE/(R\cdot g(\alpha))] - 2.315$. The fitted straight lines obtained for the IG-00 and IG-01 samples are shown in Figure 9. The calculated kinetic parameters and average activation energy of IG-00 and IG-01 are shown in Table 7.

Activation energy is the minimum energy required to transform ordinary molecules into activated molecules. The greater the activation energy, the greater the resistance to the reaction, and the more stable the substance. The average activation energies of IG-00 and IG-01 at different conversion

https://doi.org/10.1021/acsomega.3c03563
ACS Omega 2023, 8, 32752−32764

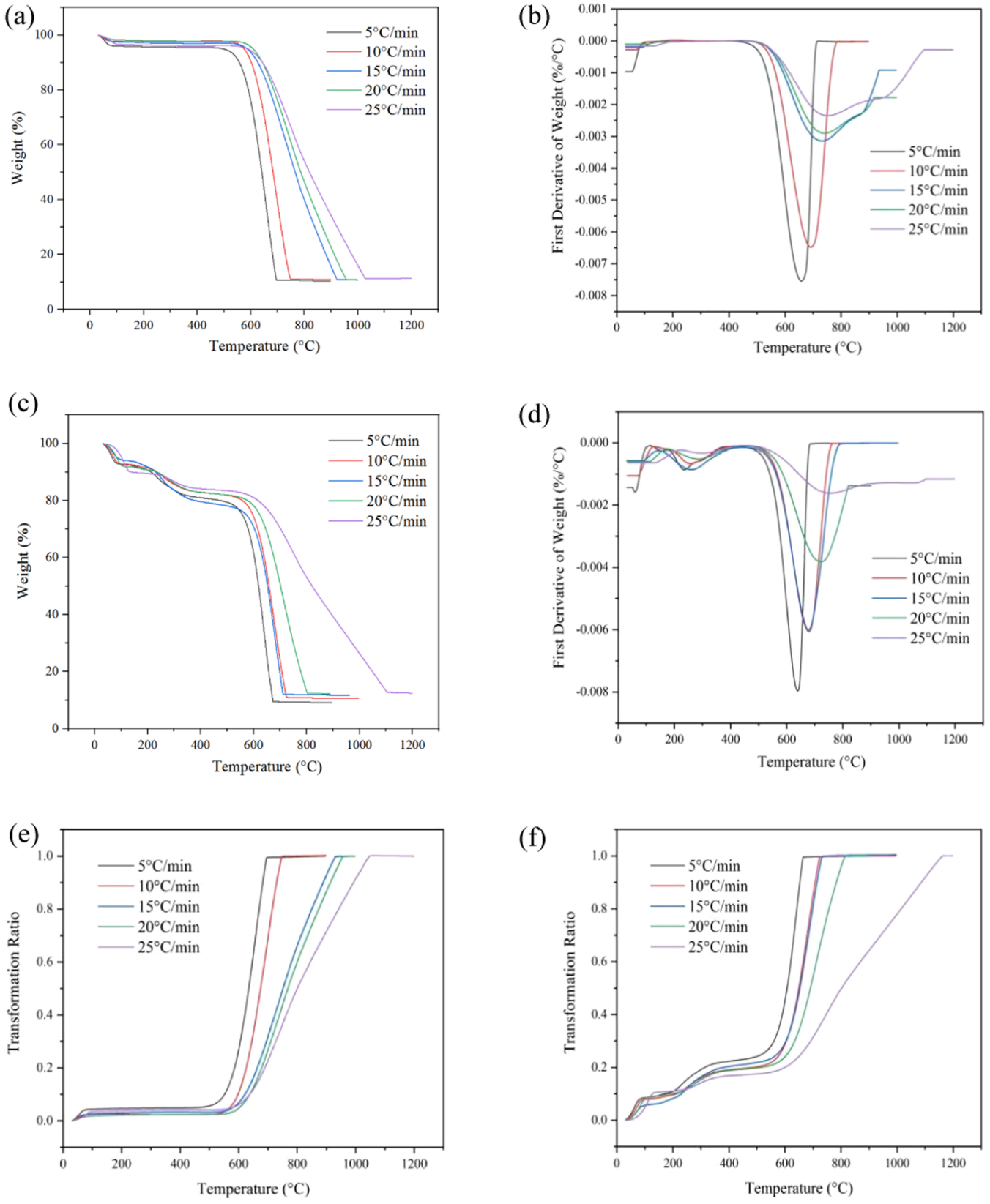

Figure 8. TG, DTG, and conversion rate curves of IG-00 and IG-01. (a) TG curves of IG-00 at different heating rates; (b) DTG curves of IG-00 at different heating rates; (c) TG curves of IG-01 at different heating rates; (d) DTG curve of IG-01 at different heating rates; (e) conversion rate curves of IG-00; and (f) conversion rate curves of IG-01.

rates are 68.4 and 103.4 kJ/mol, respectively. Based on activation energy, the thermal stability of IG-01 is greater than that of IG-00; this result is consistent with that obtained using the ignition temperature. As the conversion rate increases, the

https://doi.org/10.1021/acsomega.3c03563
ACS Omega 2023, 8, 32752−32764

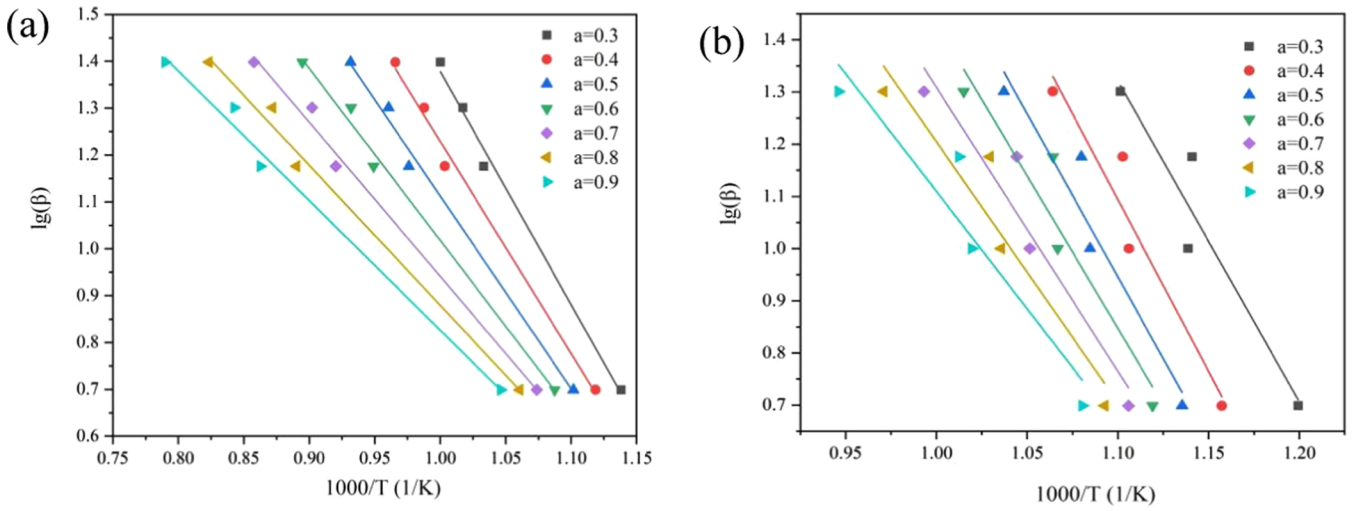

Figure 9. lg(β) and $1/T_p$ fitting lines of IG-00 and IG-01. (a) lg(β) and $1/T_p$ fitting line of IG-00 and (b) lg(β) and $1/T_p$ fitting line of IG-01.

Table 7. Nonisothermal Kinetic Parameters Calculated Using FWO

sample	conversion rate α	lg($AE/RG(\alpha)$)−2.315	−0.4567E/1000R	ideal gas constant R	standard deviation SD	activation energy (E/kJ mol^{-1})	average activation energy (E/kJ mol^{-1})
IG-00	0.3	6.4	−5.0	−0.997	0.025	90.6	68.4
	0.4	5.8	−4.5	−0.997	0.025	82.4	
	0.5	5.2	−4.1	−0.997	0.025	74.8	
	0.6	4.7	−3.7	−0.997	0.026	66.7	
	0.7	4.2	−3.3	−0.996	0.028	59.9	
	0.8	3.9	−3.0	−0.995	0.029	54.3	
	0.9	3.6	−2.8	−0.991	0.029	50.3	
IG-01	0.3	8.1	−6.2	−0.954	0.079	112.0	103.4
	0.4	8.3	−6.6	−0.965	0.069	119.8	
	0.5	7.8	−6.3	−0.963	0.070	113.8	
	0.6	7.3	−5.8	−0.952	0.080	106.4	
	0.7	6.8	−5.4	−0.961	0.072	99.1	
	0.8	6.2	−5.0	−0.953	0.079	90.9	
	0.9	5.6	−4.5	−0.048	0.083	82.0	

corresponding activation energy shows a downward trend and eventually stabilizes.

5. COMBUSTION ANALYSIS OF MODIFIED ACTIVATED CARBON

Figure 10 shows the temperature change and mass change of the IG-01 sample in the combustion test platform monitored using the thermocouple under the drying temperature of 150, 175, 180, and 210 °C.

Under the drying condition of 150 °C, the maximum temperature at the bottom of the combustion chamber was stable at approximately 169 °C and the final mass remained stable at 7.8 kg for 360 min. The activated carbon did not heat rapidly, and the maximum temperature did not exceed 500 °C (during the entire experiment), indicating that the activated carbon did not burn. Activated carbon undergoes weight loss due to the volatilization of the impregnated activated carbon solvent and water. T0−1, T0−2, and T0−3 revealed that the temperature of activated carbon at the bottom of the combustion chamber reached approximately 169 °C in the 18th min, while the temperature of T0−3 was the first to rise, followed by those of T0−1 and T0−2. The rapid temperature rise in bracket 1 occurred at the 18th min of drying (that is, when the temperature of the activated carbon at the bottom of the combustion chamber reached its highest value). The rapid temperature rise in bracket 2 began at the 76th min (that is, when the temperature in bracket 1 reached its highest value); bracket 3 started to heat up rapidly at the 140th min (that is, when the temperature in bracket 2 reached its highest value). At the 300th min, the temperature in bracket 4 reached its highest value; however, the highest temperature was only 88 °C, which was observed after no changes were observed in the activated carbon mass. Under the drying temperature of 150 °C, the heat first gathers at the bottom of the combustion chamber and then gradually transfers upward and longitudinally. The temperature increased vertically in distinct layers. The reason why the temperature in bracket 4 stabilized at 88 °C is because the fourth bracket is at the extreme end of the longitudinal temperature spread and the accumulated heat is rapidly dissipated. The temperature results monitored using thermocouples installed on each bracket show that the temperature near the center of the combustion chamber is the highest, which is followed by the temperature at the middle of the bracket. The temperature near the inner wall of the combustion chamber is the lowest, indicating that the temperature of activated carbon spreads laterally from the center to the wall of the combustion chamber during the drying process.

https://doi.org/10.1021/acsomega.3c03563
ACS Omega 2023, 8, 32752−32764

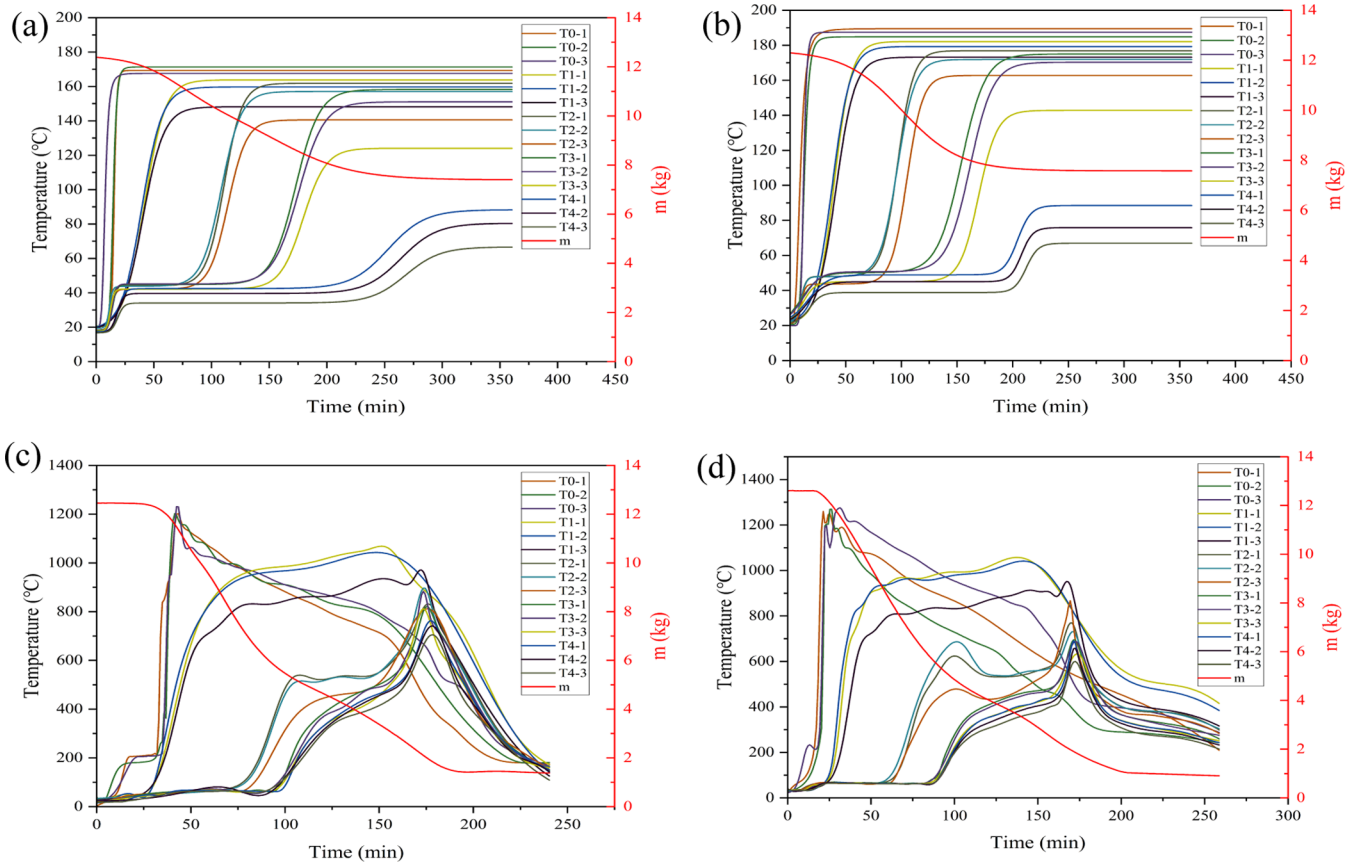

Figure 10. Activated carbon combustion curves under different drying temperatures. (a) Combustion curves of activated carbon IG-01 under 150 °C, (b) combustion curves of activated carbon IG-01 under 175 °C, (c) combustion curves of activated carbon IG-01 under 180 °C, and (d) combustion curves of activated carbon IG-01 under 210 °C.

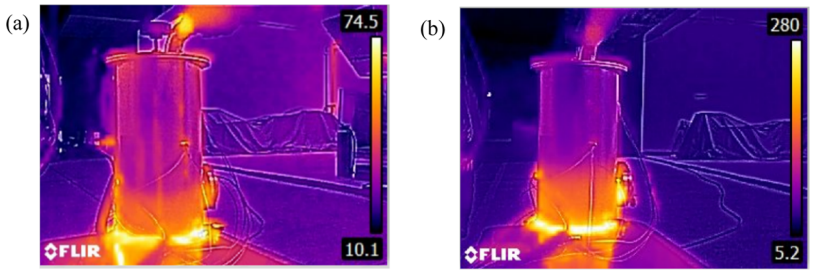

Figure 11. Thermal images captured under drying conditions of 180 °C. (a) Thermal image of activated carbon combustion at the 46th min and (b) thermal image of activated carbon combustion at the 175th min.

Under the drying temperature of 175 °C, the maximum temperature at the bottom of the combustion chamber was stable at approximately 188 °C and the final mass remained stable at 7.8 kg for 360 min. The activated carbon did not heat up rapidly, and the maximum temperature did not exceed 500 °C (during the entire experiment), indicating that the activated carbon did not burn. The combustion curve under the drying temperature of 175 °C is similar to that observed under the drying temperature of 150 °C. However, the average temperature in each bracket area under the drying temperature of 175 °C is higher than the drying temperature of 150 °C during the drying process. At the same time, the weight loss of activated carbon under a drying temperature of 175 °C was significantly faster than the drying conditions of 150 °C.

Under the drying temperature of 180 °C, the activated carbon at the bottom of the combustion chamber began to heat up rapidly at the 40th min and reached a peak temperature of 1308 °C at the 46th min. The weight of the activated carbon began to drop rapidly, and the combustion chamber began to discharge a large amount of white smoke, indicating that the activated carbon at the bottom of the combustion chamber had burned. The heat accumulated at the bottom of the combustion chamber spread vertically upward. The temperature in bracket 1 began to rise rapidly at the 30th min, reached a peak at the143th min, and then began to decline. The temperature in bracket 2 rose rapidly at the 70th and 150th min; it reached its peak value at the 175th min and then began to decrease. The temperature in brackets 3 and 4 began to rise rapidly from the 95th min, reached its peak value at the 175th min, and then began to decline. The mass of activated carbon in the combustion chamber began to stabilize and remained at 1.41 kg, and the combustion process had a tendency to end. The thermal images of activated carbon

https://doi.org/10.1021/acsomega.3c03563
ACS Omega 2023, 8, 32752−32764

combustion at the 46th and 175th min under the drying condition of 180 °C are shown in Figure 11. The trigger point of wet-modified activated carbon combustion is that activated carbon at the bottom of the combustion chamber is continuously heated by hot air, and the chemical reaction between activated carbon and oxygen generates a large amount of heat. The heat further gathers and spreads vertically upward. As a result, the temperatures in brackets 1, 2, 3, and 4 reach a maximum of 1,056, 900, 780, and 780 °C, respectively.

The combustion curve under the drying temperature of 210 °C is similar to that observed under the drying condition of 180 °C; however, the temperature of the activated carbon at the bottom of the combustion chamber keeps rising from the beginning of heating, reaches its highest value at the 25th min, and then begins to drop. The rapid rise in activated carbon temperature in bracket 1 occurred at the 25th min (that is, when the temperature of the activated carbon at the bottom of the combustion chamber rose rapidly). The temperature of activated carbon in bracket 2 rose rapidly at the 60th min, reached its peak at the 170th min, and then began to decline. The temperature in brackets 3 and 4 began to rise rapidly at the 85th min, reached its peak at the 170th min, and began to decline. The mass of activated carbon in the combustion chamber finally stabilized at 1.05 kg. The temperatures in brackets 1, 2, 3, and 4 reached a maximum value of 1,056, 900, 780, and 780 °C. This result is consistent with the highest temperature exhibited by each bracket under the drying condition of 180 °C.

Combustion experiments of modified activated carbon performed under the drying temperatures of 150, 175, 180, and 210 °C imply that the temperature that triggers the modified activated carbon combustion is between 175 and 180 °C. During activated carbon combustion, the maximum temperature in bracket 1 is higher than that in bracket 2, the maximum temperature in bracket 2 is higher than that in bracket 3, and the maximum temperatures in brackets 3 and 4 are basically the same. Similarly, as combustion progresses, the heat in the combustion chamber spreads vertically from the bottom to top. The thermocouple temperature on each bracket showed its highest value near the center of the combustion chamber and its lowest value near the inner wall of the combustion chamber, indicating that the heat is mainly gathered at the longitudinal center of the combustion chamber.

The reduction in the mass of activated carbon mainly occurs due to the evaporation of water and the solvent, which precedes the rapid temperature rise during combustion. The reduction in mass after a rapid rise in temperature mainly occurs due to a decrease in the fixed carbon content; that is, the fixed carbon reacts with oxygen to form CO and CO_2, which are discharged out of the combustion chamber along with water vapor.

6. CONCLUSIONS AND FUTURE WORK

The physicochemical properties of the activated carbon before and after modification have changed. Specifically, the specific surface area S_BET is decreased by 368 $m^2 \cdot g^{-1}$, the total volume of pore size is reduced by 0.17 $cm^3 \cdot g^{-1}$, and the content of oxygen-containing functional groups is lowered by 0.071 mmol/g compared with the untreated activated carbon. The ignition temperatures of the samples before modification were detected as 483, 596, and 599 °C, respectively. The ignition temperatures after modification were measured as 489, 607, and 611 °C, respectively. Moreover, the activation energy of the modified activated carbon increased by 35 kJ/mol compared to that of the original activated carbon. These results indicate that the modified activated carbon impregnated with the 4-amino-1,2-butanediol solution exhibits a tendency for spontaneous combustion lower than that of the activated carbon before modification.

The combustion experiments on activated carbon were conducted by using a self-designed combustion platform. It was observed that the modified activated carbon undergoes combustion when subjected to drying temperatures between 175 and 180 °C. When compared to the drying condition of 180 °C, elevating the drying temperature to 210 °C caused the activated carbon at the bottom of the combustion chamber to reach its peak temperature 21 min earlier, and the residual mass of activated carbon after combustion was reduced by an additional 0.36 kg. Thermocouples positioned on each bracket indicated that the highest temperature was recorded near the center of the combustion chamber, while the lowest temperature was measured near the inner wall. This observation suggests that heat predominantly accumulates at the longitudinal center of the combustion chamber.

Based on the industrial engineering application requirements of modified activated carbon in different scenarios, there are many solvents used for the modification of activated carbon, and the activated carbon modified by different solvents may show different thermal stability. In our future work, we try to build a database to collect the data for the comparison of the activated carbon before and after modification in terms of ignition temperature and activation energy and explore the drying temperatures that trigger the combustion of activated carbon modified with different solvents via a combustion test platform to realize practical industrial applications on activated carbon modification.

AUTHOR INFORMATION

Corresponding Author

Bing J. Zhang − *School of Materials Science and Engineering, Guangdong Engineering Center for Petrochemical Energy Conservation, The Key Laboratory of Low-carbon Chemistry & Energy Conservation of Guangdong Province, Sun Yat-Sen University, Guangzhou 510006, P. R. China;* orcid.org/0000-0001-9830-9193; Email: zhbingj@mail.sysu.edu.cn

Authors

Qing-en Li − *School of Materials Science and Engineering, Guangdong Engineering Center for Petrochemical Energy Conservation, The Key Laboratory of Low-carbon Chemistry & Energy Conservation of Guangdong Province, Sun Yat-Sen University, Guangzhou 510006, P. R. China*

Shu-shen Lyu − *School of Materials Science and Engineering, Guangdong Engineering Center for Petrochemical Energy Conservation, The Key Laboratory of Low-carbon Chemistry & Energy Conservation of Guangdong Province, Sun Yat-Sen University, Guangzhou 510006, P. R. China;* orcid.org/0000-0001-8919-0776

Zhiwen Qi − *Max Planck Partner Group at the State Key Laboratory of Chemical Engineering, School of Chemical Engineering, East China University of Science and Technology, Shanghai 200237, P. R. China;* orcid.org/0000-0003-2037-2234

Complete contact information is available at: https://pubs.acs.org/10.1021/acsomega.3c03563

https://doi.org/10.1021/acsomega.3c03563
ACS Omega 2023, 8, 32752−32764

Notes

The authors declare no competing financial interest.

■ ACKNOWLEDGMENTS

This research is supported by the National Natural Science Foundation of China (No. 21978330).

■ REFERENCES

(1) Kang, Y.-J.; Jo, H.; Jang, M.; Ma, X.; Jeon, Y.; Oh, K.; Park, J. A Brief Review of Formaldehyde Removal through Activated Carbon Adsorption. *Appl. Sci.* **2022**, *12*, No. 5025, DOI: 10.3390/app12105025.

(2) Kang, Y.-J.; Jo, H.; Jang, M.; Han, G.; Yoon, S.; Oh, K.; Park, J. Acid treatment enhances performance of beads activated carbon for formaldehyde removal. *Carbon Lett.* **2023**, *33*, 397−408.

(3) Ryu, D.-Y.; Kim, D.; Kang, Y.; Lee, Y.; Nakabayashi, K.; Miyawaki, J.; Park, J.; Yoon, S. Preparation of environmental-friendly N-rich chitin-derived activated carbon for the removal of formaldehyde. *Carbon Lett.* **2022**, *32*, 1473−1479, DOI: 10.1007/s42823-022-00379-x.

(4) Isinkaralar, K.; Gullu, G.; Turkyilmaz, A. Experimental study of formaldehyde and BTEX adsorption onto activated carbon from lignocellulosic biomass. *Biomass Convers. Biorefin.* **2022**, *13*, 4279−4289, DOI: 10.1007/s13399-021-02287-y.

(5) Zhu, L.; Shen, D.; Luo, K. A critical review on VOCs adsorption by different porous materials: Species, mechanisms and modification methods. *J. Hazard. Mater.* **2020**, *389*, No. 122102.

(6) Saqlain, S.; Zhao, S.; Kim, S.; Kim, Y. Enhanced removal efficiency of toluene over activated carbon under visible light. *J. Hazard. Mater.* **2021**, *418* (11), No. 126317.

(7) Wang, J.; Cao, W.; Wei, W.; Jin, H. Adsorption characteristic analysis of PAHs on activated carbon with different functional groups by molecular simulation. *Environ. Sci. Pollut. Res.* **2023**, *30*, 32452−32463.

(8) Demiral, I.; Samdam, C.; Demiral, H. Enrichment of the surface functional groups of activated carbon by modification method. *Surf. Interfaces* **2021**, *22* (14), No. 100873.

(9) Bhatnagar, A.; Hogland, W.; Marques, M.; Sillanpää, M. An overview of the modification methods of activated carbon for its water treatment applications. *Chem. Eng. J.* **2013**, *219*, 499−511.

(10) Bazan-Wozniak, A.; Cielecka-Piontek, J.; Nosal-Wiercinska, A.; Pietrznak, R. Adsorption of Organic Compounds on Adsorbents Obtained with the Use of Microwave Heating. *Materials* **2022**, *15*, No. 5664, DOI: 10.3390/ma15165664.

(11) Zhang, D.; Zhang, M.; Ding, F.; Liu, W.; Zhang, L.; Cui, L. Efficient removal of formaldehyde by polyethyleneimine modified activated carbon in a fixed bed. *Environ. Sci. Pollut. Res.* **2020**, *27*, 18109−18116.

(12) Shalbafan, A.; Hassannejad, H.; Rahmaninia, M. Formaldehyde adsorption capacity of chitosan derivatives as bio-adsorbents for wood-based panels. *Int. J. Adhes. Adhes.* **2020**, *102*, No. 102669.

(13) Rong, X.; Cao, Q.; Gao, Y.; Du, X.; Dou, H.; Yan, M.; Li, S.; Wang, Q.; Zhang, Z.; Chen, B. Performance optimization and kinetic analysis of HNO_3. *Front. Enery Res.* **2023**, *10*, No. 1047254, DOI: 10.3389/fenrg.2022.1047254.

(14) Belyaeva, O. V.; Krasnova, T.; Semenova, S. Effect of modification of granulated activated carbons with ozone on their properties. *Russ. J. Appl. Chem.* **2011**, *84*, 597−601.

(15) Wang, S.; Sun, H.; Ang, H.; Tade, M. Adsorptive remediation of environmental pollutants using novel graphene-based nanomaterials. *Chem. Eng. J.* **2013**, *226*, 336−347.

(16) Abdulrasheed, A.; Jalil, A.; Triwahyono, S.; Zaini, M.; Gambo, Y.; Ibrahim, M. Surface modification of activated carbon for adsorption of SO_2 and NOx: A review of existing and emerging technologies. *Renewable Sustainable Energy Rev.* **2018**, *94*, 1067−1085.

(17) Wang, J.; Zhang, Q.; Deng, M. Eco-Friendly Preparation of Biomass-Derived Porous Carbon and Its Electrochemical Properties. *ACS Omega* **2022**, *7* (26), 22689−22697.

(18) Suresh, S.; Bandosz, T. J. Removal of formaldehyde on carbon-based materials: a review of the recent approaches and findings. *Carbon* **2018**, *137*, 207−221.

(19) Ding, L.; Khan, F.; Ji, J. Risk-based safety measure allocation to prevent and mitigate storage fire hazards. *Process Saf. Environ. Prot.* **2020**, *135*, 282−293.

(20) Altarawneh, S.; Mohammad, A.; Chris, D.; Adam, B.; Sam, K. Thermodynamic, pyrolytic, and kinetic investigation on the thermal decomposition of polyvinyl chloride in the presence of franklinite. *Process Saf. Environ. Prot.* **2022**, *168*, 558−569.

(21) Pritam, K.; Nandi, B. K. Assessment of combustion characteristics of high ash Indian coal, petroleum coke and their blends for cement industry using TGA. *Clean. Chem. Eng.* **2023**, *5*, No. 100091, DOI: 10.1016/j.clce.2022.100091.

(22) Xu, Q.; Yang, S.; Yang, W.; Tang, Z.; Song, W.; Zhou, B.; Jiang, X. Effect of particle size and low-temperature secondary oxidation on the active groups in coal structures. *Process Saf. Environ. Prot.* **2021**, *149*, 334−344.

(23) Han, Q.; Cui, C.; Jiang, S.; Deng, C.; Jin, Z. Effect of Water Evaporation on the Inhibition of Spontaneous Coal Combustion. *ACS Omega* **2022**, *7* (8), 6824−6833.

(24) Zhang, X.; Yu, C.; Chen, G.; Gao, F.; Lu, B.; Zou, J. Study on the Mechanism of Antioxidants Affecting the Spontaneous Combustion Oxidation of Coal. *ACS Omega* **2023**, *8* (3), 3396−3403, DOI: 10.1021/acsomega.2c07273.

(25) Onifade, M.; Genc, M. Spontaneous combustion liability of coal and coal-shale: A review of prediction methods. *Int. J. Coal Sci. Technol.* **2019**, *6*, 151−168.

(26) Abdulsalam, J.; Mulopo, J.; Bada, S.; Oboirien, B. Natural gas storage properties of adsorbents synthesized from three different coal waste in South Africa. *Fuel* **2020**, *267*, No. 117157.

(27) Nugroho, Y.; Mcintosh, A.; Gibbs, B. Low-temperature oxidation of single and blended coals. *Fuel* **2000**, *79*, 1951−1961.

(28) Jia, X.; Wu, J.; Lian, C.; Wang, J.; Rao, J.; Feng, R.; Chen, Y. Investigating the effect of coal particle size on spontaneous combustion and oxidation characteristics of coal. *Environ. Sci. Pollut. Res.* **2022**, *29*, 16113−16122.

(29) Ma, T.; Zhai, X.; Xiao, Y.; Bai, Y.; Shen, K.; Song, B.; Hao, L.; Ren, L.; Chen, X. Study on the influence of key active groups on gas products in spontaneous combustion of coal. *Fuel* **2023**, *344*, No. 128020.

(30) Niu, Z.; Liu, G.; Yin, H.; Wu, D.; Zhou, C. Investigation of mechanism and kinetics of non-isothermal low temperature pyrolysis of perhydrous bituminous coal by in-situ FTIR. *Fuel* **2016**, *172*, 1−10.

(31) Jayabalan, T.; Pré, P.; Héquet, V.; Cloirec, P. Statistical quantification of the influence of material properties on the oxidation and ignition of activated carbons. *Adsorption* **2008**, *14* (4−5), 679−686.

(32) Xu, Q.; Yang, S.; Cai, J.; Zhou, B.; Xin, Y. Risk forecasting for spontaneous combustion of coals at different ranks due to free radicals and functional groups reaction. *Process. Saf. Environ. Prot.* **2018**, *118*, 195−202.

(33) Tang, Y.; Wang, H. Experimental investigation on microstructure evolution and spontaneous combustion properties of secondary oxidation of lignite. *Process Saf. Environ. Prot.* **2019**, *124*, 143−150.

(34) Zhang, Y.; Zhou, J.; Deng, J.; Wen, X.; Liu, C.; Wang, A.; Shu, P. Heat Release Characteristic of Key Functional Groups during Low-Temperature Oxidation of Coal. *Combust. Sci. Technol.* **2020**, *193* (15), 2692−2703, DOI: 10.1080/00102202.2020.1755970.

(35) Guo, J.; Zhang, T.; Pan, H. Study on the Variations of Key Groups and Thermal Characteristic Parameters during Coal Secondary Spontaneous Combustion. *ACS Omega* **2023**, *8* (4), 4176−4186.

(36) Gao, Y.; Qin, B.; Shi, Q.; Liang, H.; Chen, K. Effect of Igneous Intrusions on Low-temperature Oxidation Characteristics of Coal in Daxing Mine, China. *Combust. Sci. Technol.* **2021**, *193*, 577−593.

(37) Yang, F.; Lai, Y.; Song, Y. Determination of the influence of pyrite on coal spontaneous combustion by thermodynamics analysis. *Process. Saf. Environ. Prot.* **2019**, *129*, 163−167.

https://doi.org/10.1021/acsomega.3c03563
ACS Omega 2023, 8, 32752−32764

(38) Guo, W.; Zhang, C.; Han, Y. Study the effect of drying on the oxidation thermogravimetric and functional group composition characteristics of immersed lignite. *Sci. Rep.* **2022**, *12* (1), No. 2164.
(39) Zhang, Y.; Chen, L.; Zhao, J.; et al. Evaluation of the spontaneous combustion characteristics of coal of different metamorphic degrees based on a temperature-programmed oil bath experimental system. *J. Loss Prev. Process Ind.* **2019**, *60*, 17−27.
(40) Du, W.; Zhang, J.; Xie, Q.; et al. Experimental study on optimizing the inhibition effect of pre-injection inhibitor on coal spontaneous combustion. *Energy Sources, Part A* **2020**, 1−18.
(41) Ma, D.; Qin, B.; Gao, Y.; Jiang, J.; Feng, B. An experimental study on the methane migration induced by spontaneous combustion of coal in longwall gobs. *Process Saf. Environ. Prot.* **2021**, *147*, 292−299.
(42) Zhu, J.; Liu, Z.; Cao, Z.; Han, X.; Hao, L.; Wei, H. Development of a general inherent safety assessment tool at early design stage of chemical process. *Process Saf. Environ. Port.* **2022**, *167*, 356−367.
(43) Lin, H.; Luan, H.; Yang, L.; Han, C.; Karampour, H.; Chen, G. A safety assessment methodology for thermo-mechanical response of offshore jacket platform under fire. *Process Saf. Environ. Prot.* **2022**, *160*, 184−198.
(44) Malendowski, M.; Glema, A. Development and implementation of coupling method for CFD-FEM analyses of steel structures in natural fire. *Procedia Eng.* **2017**, *172*, 692−700.
(45) Shibani; Salehi, F.; Baalisampang, T.; Abbassi, R. Numberical modeling towards the safety assessment of multiple fires in confined areas. *Process Saf. Environ. Prot.* **2022**, *160*, 594−609, DOI: 10.1016/j.psep.2022.02.057.
(46) Masawat, N.; Atong, D.; Sricharoenchaikul, V. Thermo-kinetics and product analysis of the catalytic pyrolysis of Pongamia residual cake. *J. Environ. Manage.* **2019**, *242*, 238−245.

https://doi.org/10.1021/acsomega.3c03563
ACS Omega 2023, 8, 32752−32764